energies

MDPI

Article

Dicyanovinyl and Cyano-Ester Benzoindolenine Squaraine Dyes: The Effect of the Central Functionalization on Dye-Sensitized Solar Cell Performance

Simone Galliano [1], Vittoria Novelli [2,3], Nadia Barbero [1,*], Alessandra Smarra [1], Guido Viscardi [1], Raffaele Borrelli [4], Frédéric Sauvage [2,3,*] and Claudia Barolo [1]

1 NIS and INSTM Reference Centre, Department of Chemistry, University of Torino, Via Pietro Giuria 7, Torino 10125, Italy; simone.galliano@unito.it (S.G.); cuscuta@virgilio.it (A.S.); guido.viscardi@unito.it (G.V.); claudia.barolo@unito.it (C.B.)

2 Laboratoire de Réactivité et Chimie du Solide (UMR-CNRS 7314), Université de Picardie Jules Verne, 33 Rue Saint-Leu, Amiens Cedex 80039, France; vittoria.novelli@u-picardie.fr

3 Institut de Chimie de Picardie (FR CNRS 3085), Amiens Cedex 80039, France

4 Dipartimento di Scienze Agrarie, Forestali e Alimentari, University of Torino, Largo Paolo Braccini 2, Grugliasco 10095, Italy; raffaele.borrelli@unito.it

* Correspondence: nadia.barbero@unito.it (N.B.); frederic.sauvage@u-picardie.fr (F.S.); Tel.: +39-011-670-7597 (N.B.); +33-3-2282-7971 (F.S.)

Academic Editor: Tapas Mallick
Received: 12 April 2016; Accepted: 17 June 2016; Published: 23 June 2016

Abstract: In order to achieve a greater light absorption in the near-infrared (NIR) region with a panchromatic spectral response and to suppress the photo-isomerisation phenomenon, we herein report the design, synthesis, spectroscopic and electrochemical characterization of novel centrally functionalized symmetric benzoindolenine squaraine dyes. These molecules have shown different photoelectrical conversion properties, depending on the dicyanovinyl and cyano-ester group substitution on the squaric core unit and on the extension of the π-conjugation.

Keywords: dye-sensitized solar cells; NIR-sensitizers; squaraines; central functionalization

1. Introduction

Dye-sensitized Solar Cells (DSCs) are a promising alternative to conventional photovoltaics, thanks to their intrinsic low-cost and easy manufacturing procedures. Although the efficiencies are still limited if compared to crystalline Si-based devices, recently a new record efficiency exceeding 14% has been reported by making use of metal-free organic dyes [1].

In DSCs, one of the most critical components is the sensitizer which is responsible for the light harvesting and the charge separation process, namely electron injection into the semiconductor oxide and dye regeneration with hole transfer to the redox mediator. The extension of light absorption capability by the dye appears to be one of the most critical factors to achieve higher solar-to-electricity power conversion efficiencies (PCEs). The design of efficient sensitizers combining high molar extinction coefficients and a panchromatic spectral response, from visible to near-IR (NIR) wavelengths, is so far a grail not yet achieved. Extending optical absorption of the metal to ligand charge transfer (MLCT) band towards the NIR region has been achieved on metal-organic Ru-based dyes [2,3], as well as for fully organic dyes with similar behavior [4].

The advantages in the use of organic dyes stem from their higher molar extinction coefficients, tunable absorption properties and lower-cost synthesis. Many different classes of organic sensitizers have been studied, among them thiophene, triarylamine and carbazole-based dyes showed excellent

capabilities to efficiently convert sunlight, despite their absorption being limited to the visible region [1,5,6]. To achieve a higher harvesting of NIR wavelengths, polymethine dyes represent a better choice [7]. Among these, squaraine dyes are particularly promising as sensitizers with good thermal and chemical stability. Their peculiar structure paves the way to a large versatility in molecular modification leading to sharp and intense absorption bands which can be tuned from the visible towards the NIR region [8]. The basic squaraine structure is formed by a cyclobuten-2,4-dione core conjugated in position 1,3 with two electron-donor aromatic moieties. This molecular elongation allows to extend the π-conjugation and to achieve visible-NIR light absorption (600–800 nm).

Squaraine dyes particularly suffer from photo-isomerization between *cis*- and *trans*-configurations. It occurs through a twisted intramolecular charge transfer (TICT) process that yields a non-radiative decay of the dye excited state, hampering quantitative fast electron injection and consequently limiting the cell efficiency [9]. Different strategies were proposed to block the photoisomerization mechanism in these structures: the doubling of anchoring moieties, the insertion of long alkyl chains on the lateral groups or the functionalization of the squaric core unit [10–12].

The first strategy implies the addition of a second anchoring group that provides a stronger electronic coupling with the semiconductor surface, a greater stability and a decrease in HOMO-LUMO energy levels contributing to a slight bathochromic shift of the spectral response of the sensitizer as in the case of VG1 dye [10]. The insertion of long alkyl chains, such as octyl on benzoindolenine moieties prevents the intramolecular rotation owing to the increased steric hindrance. This was demonstrated by NMR analysis showing the presence of more than one conformer in solution on the timescale of the experiment. As a result, 6.1% power conversion efficiency was obtained for VG10-C8 dye [11]. Interestingly, the modification of the squaric core, first proposed by Beverina et al., appears as a promising alternative strategy to lock the structure into the *cis*-configuration [12]. This was accomplished by the introduction of an electron withdrawing diethylthiobarbituric moiety on the *core* unit. Moreover, this moiety induces a slight bathochromic shift of the maximum absorption and the occurrence of a second absorption band at higher energies (450 nm). Similar observations were made on other electron withdrawing groups, in particular with the dicyanovinyl group. This group causes a red-shifting of the absorption maximum of about 50 nm, together with the appearance of a second absorption peak at around 380–400 nm, yielding a 30% increase in PCE [13–15]. A greater bathochromic shift has been reported by Han's group on a new series of squaraines centrally functionalized with a cyano-ester moiety [16,17]. Accordingly to these strategies, better performances are obtained with symmetrical dianchored squaraines centrally substituted with an electron withdrawing group as reported by Maeda et al. [13] (η = 3.6%) and Qin et al. [16] (η = 5.66%).

In order to achieve a greater light absorption in the NIR region with a panchromatic spectral response, we combined the three aforementioned strategies exploiting symmetrical structures bearing long C8 alkyl chains with the functionalization of the central *core* unit. Therefore, we present in this work the design, synthesis and characterization of four novel central functionalized squaraine dyes (VG2-C8, VG3-C8, VG11-C8 and VG12-C8), shown in Figure 1.

In particular, starting from two analogous squaraines reported in literature (SQM1a [13] and HSQ4 [16]), we conceived the VG2-C8 dye, with longer alkyl chains, and the VG3-C8 dye, with butyl-ester groups, respectively. Then, thanks to our previous results with VG1-C8 [10] and VG10-C8 [11] dyes, we also prepared two new benzo-derivative analogs VG11-C8 and VG12-C8. Actually, VG2-C8 and VG11-C8 have a strong electron-withdrawing dicyanovinyl group on the squaric acid core while VG3-C8 and VG12-C8 bear a cyano-butyl-ester substituent. Since the latter substituent is less electron withdrawing than –CN, we expect that it might raise the energy levels of both HOMO and LUMO. All four synthesized dyes should present a new locked *cis*-configuration, which should hinder the photoisomerization and, consequently, improve the DSCs' performance.

Henceforward for simplicity and better readability of this text, the VG-series squaraines will be simply called with their short name (VGx), omitting the chain length (C8) that is the same for all the

dyes. Previous results obtained for the reference compounds VG1 and VG10 are reported in some sections for comparison.

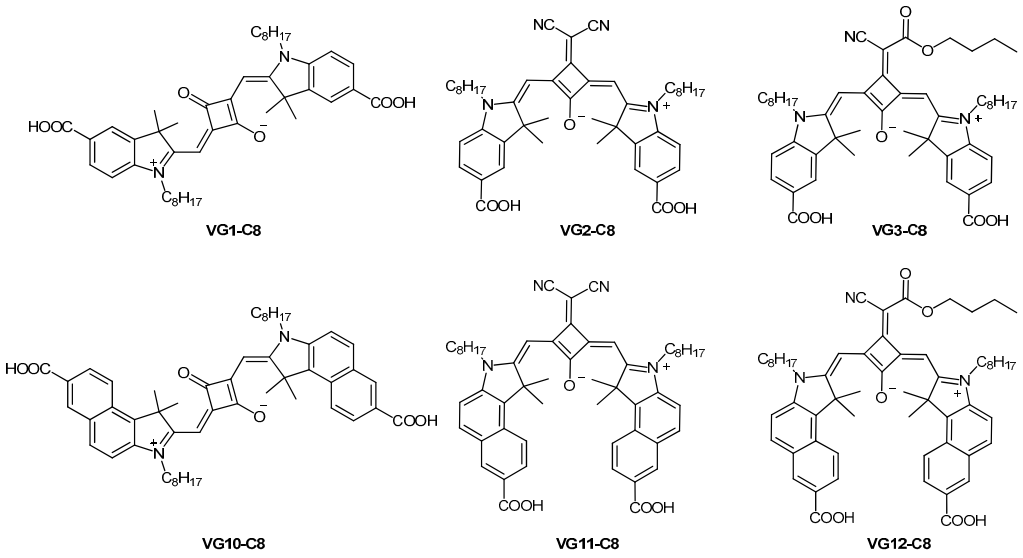

Figure 1. Structures of the four synthesized squaraines (VG2-C8, VG3-C8, VG11-C8, VG12-C8) and of VG1-C8 and VG10-C8 as a comparison.

2. Results

2.1. Synthesis

The four central substituted squaraine dyes were prepared by a microwave-assisted method recently developed for squaraine dyes [18], as shown in Figure 2. The synthesis of VG2 and VG11 consists of a condensation reaction between a dicyanovinyl substituted squaric acid derivative 1 and a quaternarized indolenine 3 or benzoindolenine 4 to get the aforementioned squaraines. If the synthetic procedure for the dicyanovinyl substituted squaraines is a well-established method [13,19,20] which has been recently improved by microwave irradiation [18], the synthetic pathway to obtain the two cyano-ester dyes is a modification of what has been reported in literature for similar central functionalized squaraines [16,17,21].

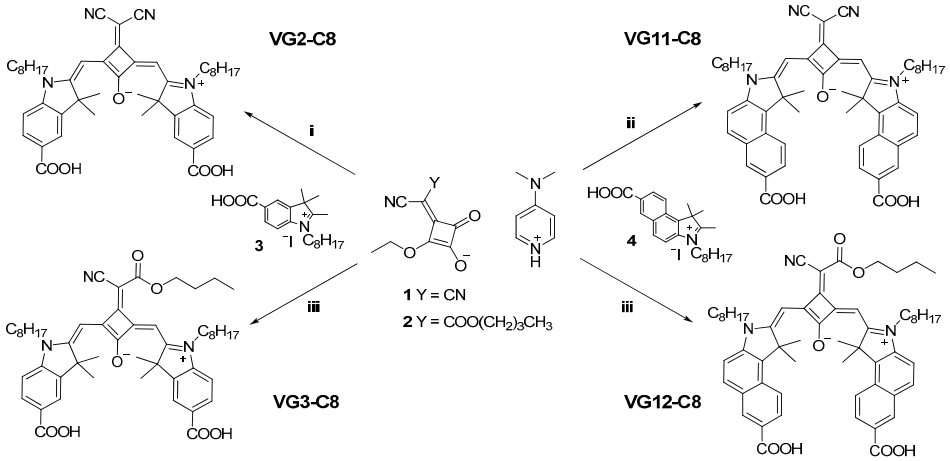

Figure 2. Synthesis of VG2-C8, VG3-C8, VG11-C8 and VG12-C8 dyes. *Experimental conditions*: (i) toluene/BuOH, MW, 30 min, 155 °C; (ii) pyridine/BuOH, MW, 15 min, 155 °C; (iii) toluene/BuOH, MW, 15 min, 155 °C.

The complete synthetic procedures are reported in Figure S1 (Supplementary Materials) as well as ^{1}H NMR of intermediates 1 and 2 and of the four squaraines which are reported in Figures S2–S7 (Supplementary Materials).

Actually, for VG3 and VG12 we used the same synthetic approach used for the previously reported symmetrical dicyanovinyl squaraines VG2 and VG11 (Figure S1, see Supplementary Materials). For this, in the condensation reaction, a cyano-ester substituted squaric acid derivative 2 was used instead of intermediate 1. This allowed us to reduce the number of synthetic steps (i.e., avoiding the formation of the intermediate). Moreover, it is worth mentioning that, as previously reported by Tatarets et al. [21], the condensation reaction for the squaraine formation is performed in a toluene/butanol mixture using a cyano-butyl-ester. When performing the reaction using a cyano-ethyl-ester in butanol, a mixture of the cyano-ethyl and cyano-butyl compounds was obtained by us, in contrast to what Han's group has previously reported [16,17].

2.2. Optical Properties

As shown in Figure 3, the four squaraines exhibit intense and sharp absorptions in the far-red region. Their molar extinction coefficient is lower than the analogous unsubstituted VG1-C8 ($\log\varepsilon = 5.53$) and VG10-C8 ($\log\varepsilon = 5.46$). This can be explained by a computational analysis. The $S_0 \rightarrow S_1$ transition in VG1/VG10 and VG2/VG3/VG11/VG12 can be described as HOMO-LUMO transitions. In these latter however the HOMO orbital has a strong contamination from the central substituent which completely disappears in the LUMO; this lowers the overlap of the two orbitals, and is probably the main cause of the reduced overall intensity of the transition. The substitution on the central squaric ring with the strong electron-withdrawing dicyanovinyl group gives rise to a red shift of about 40–45 nm coming with a hypochromic effect. The cyano-ester insertion is responsible of a further red-shift of about 5–8 nm. It is worth noting that these new central functionalized squaraines show two main absorption bands, one in the long-wavelength region and another, less intense, in the blue region, which are assigned to the S_1 and S_2 transitions, respectively [20].

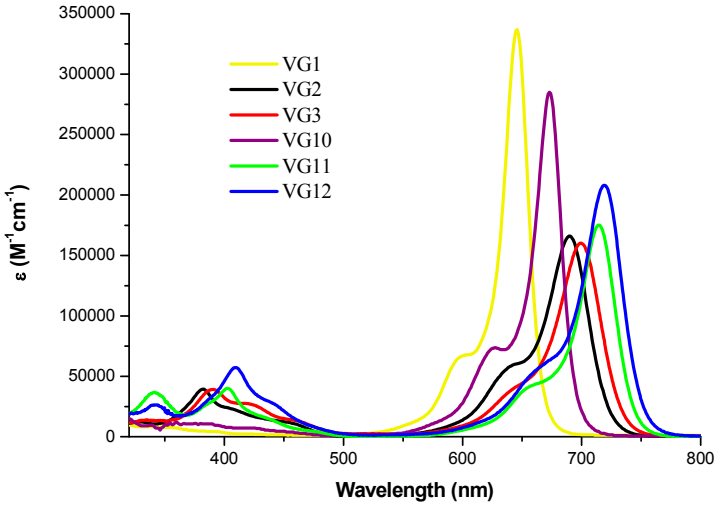

Figure 3. Absorption spectra of VG1-C8, VG2-C8, VG3-C8, VG10-C8, VG11-C8 and VG12-C8 in ethanol.

Extending the π-conjugation by replacing the indolenine with a benzoindolenine (VG1 → VG10, VG2 → VG11 and VG3 → VG12) affords a further bathochromic shift of about 20 nm. UV-Vis absorption and steady-state fluorescence emission spectra show a negative solvatochromism which accounts for a higher polarity of the ground state with respect to the excited state. A detailed description of the spectroscopic characterization as well as the complete results on absorbance and fluorescence are reported in the Supplementary Materials (Tables S1–S3).

2.3. Electrochemical Properties

The ground-state oxidation (E_{ox}) and reduction (E_{red}) potentials of the new symmetrical dyes were evaluated by cyclic voltammetry (CV, see Figure S8). By means of CV measurement, it is possible to extract the energy levels of the frontier molecular orbitals (HOMO and LUMO) of dyes. In particular, the E_{ox} potential corresponds to HOMO energy level, while, with a larger approximation, the E_{red} potential refers to LUMO level. For this reason, we chose to calculate LUMO levels as the difference between HOMO (E_{ox}) and the optical band gap $\Delta E_{0\text{-}0}$ (obtained from spectroscopic characterization and reported in Table S2). HOMO and LUMO levels of the novel central-substituted squaraines are reported in Figure 4, with the unsubstituted VG1 and VG10 dyes as a comparison. In Figure 4, the measured E_{red} potentials of each dye are also reported.

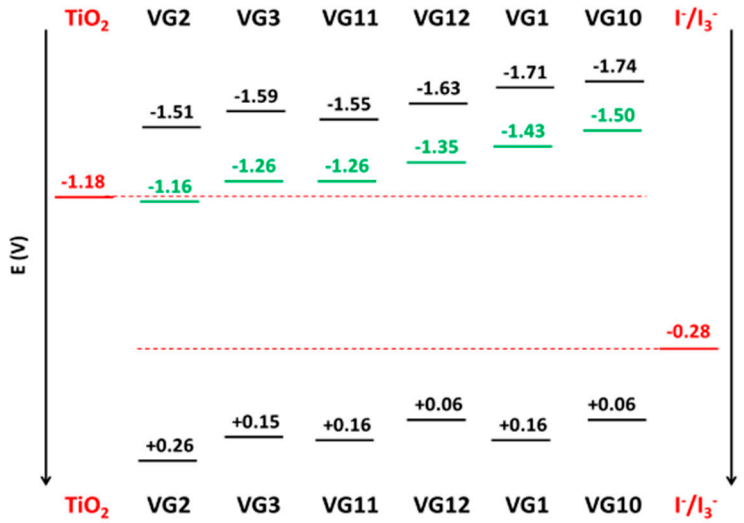

Figure 4. HOMO and LUMO energy levels (black) and E_{red} potentials (green) of the four novel squaraine dyes vs. Fc/Fc^+ (in V); VG1 and VG10 dyes are reported as a comparison [11].

VG2, VG3, VG11 and VG12 dyes exhibited the first oxidation potentials at 0.26, 0.15, 0.16, and 0.06 V (vs. Fc/Fc^+), respectively. The measured HOMO levels are positive enough to have energetically favorable dye regeneration by iodide species (−0.28 V) [11]. On the other hand, the LUMO levels of VG2, VG3, VG11 and VG12 dyes are −1.51, −1.59, −1.55 and −1.63 V (vs. Fc/Fc^+), respectively. These values seem to be enough negative to allow an efficient electron injection by the excited dye in the conduction band of TiO_2 (−1.18 V).

Looking at the molecular structure of the different dyes, it is clear that the E_{ox} and E_{red} potentials are negatively shifted by replacing the indolenine with a benzoindolenine moiety, in good agreement with our previous work on VG1 and VG10 dyes [11]. On the contrary, central substitutions positively move the potentials, stabilizing the molecular orbitals, and the effect increases in going from a cyano-ester to a dicyanovinyl group. This latter evidence demonstrates that the electron withdrawing effect of the central substitution tends to stabilize the molecular energy levels, particularly for E_{red}, leading to a more efficient dye regeneration, but worse electron injection.

2.4. Computational Investigation

In order to rationalize the spectroscopic properties of the functionalized squaraines, their electronic transitions have been characterized by means of quantum chemical calculations based on the time-dependent density functional theory (TD-DFT). In particular, the two cyano-butyl-ester squaraines have been processed like the cyano-methyl-ester analogs in order to simplify the computational calculations. Vertical transitions energies of the four molecules are reported in Table S4 (see Supplementary Materials). We point out that whereas the dyes can certainly exist in different

configurations, previous computational analyses on squaraines suggest that different isomers have very similar electronic spectra [11,22]. The predicted first excitation energies are about 0.3 eV higher than the experimental data, confirming a similar trend than previous reports on TD-DFT [11,22–24].

The $S_0 \rightarrow S_1$ transition in both dicyanovinyl and cyano-ester substituted squaraines involves a HOMO-LUMO excitation and has a partial intramolecular charge-transfer character. The HOMO orbital has a non-negligible contribution from the dicyanovinyl/cyano-ester group, which is lacking in the LUMO (see Figure S9).

TD-DFT calculations also predict relatively large oscillator strengths for the S_0/S_2, S_0/S_3 and S_0/S_4 of the four dyes in the range 320–340 nm, which can be ascribed to the observed band at around 400 nm. As aforementioned, the intensity of this band is comparatively much higher in the case of the centrally functionalized squaraines. The calculations point out that they involve strongly localized orbitals located on the central substituent (Figure S9).

We can also notice that the computed $S_0 \rightarrow S_1$ transitions of the cyano-ester substituted squaraines show a small bathochromic shift with respect to its analogous dicyanovinyl (Table S3). This is in excellent agreement with the experimental data.

2.5. Photovoltaic Performances

The performances of these new squaraine structures were optimized using a traditional double layer geometry of anatase TiO_2 photo-anode, composed of ca. 8 µm thickness of 20 nm-based TiO_2 nanoparticles sheltered with ca. 5 µm thick scattering layer of 400 nm particles to back-reflect unabsorbed photons towards the nanoparticles. To gain better insight on the effect of the substitution on the squaric central core and the effect of the π-conjugation enhancement in the excited state acceptor units, the J-V curves recorded for each of the four dyes, with the analogous unsubstituted VG1 and VG10, under standard A.M. 1.5G irradiation conditions, are gathered in Figure 5a.

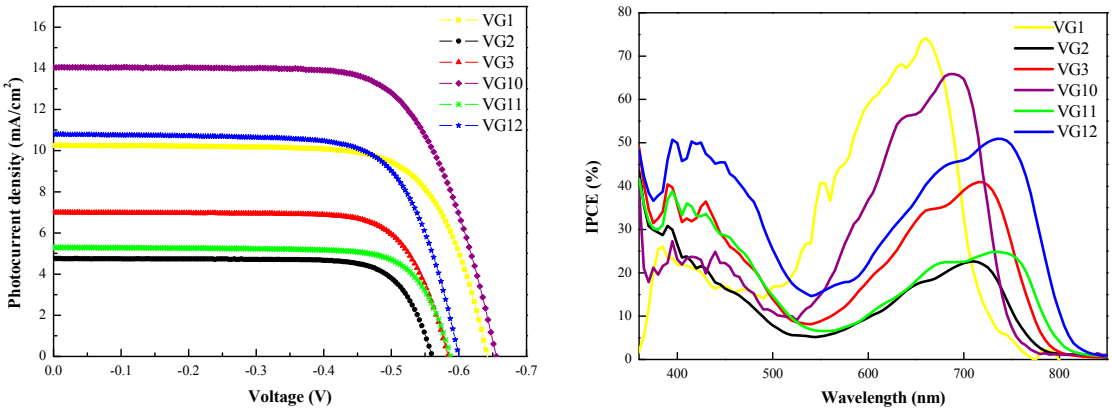

Figure 5. (**a**) J-V curves recorded under standard A.M. 1.5G condition for VG2-C8, VG3-C8, VG11-C8 and VG12-C8 squaraine dyes (VG1-C8 and VG10-C8 are reported as a comparison); (**b**) the corresponding action spectra of the devices.

The key photovoltaic parameters extracted are tabulated in Table 1. Based on this comparison, one can conclude that the substitution on the squaric core with a strong electron withdrawing dicyanovinyl group (VG2 black and VG11 green curves) has a negative effect on the photovoltaic performance since both the photovoltage and photocurrent decrease (compared with the unsubstituted VG1, yellow curve, and VG10, purple curve). On the contrary, a positive effect is registered when the dicyanovinyl group is substituted by a cyano-butyl-ester group (VG3 red and VG12 blue curves), which leads not only to an increment of the photovoltage but also of the photocurrent, with a noticeable final improvement in the power conversion efficiency. On the other hand, increasing

the π-conjugation of the electron withdrawing unit also improves the performances when comparing benzoindolenine- (VG11 and VG12) with indolenine-based squaraines (VG2 and VG3). Consequently, the best performing dye of this novel series is the benzoindolenine-based VG12 structure for which we obtained an overall power conversion efficiency of 4.6%, with a J_{sc} = 10.8 mA/cm^2, V_{oc} = 599 mV and ff = 71%. The power conversion efficiency achieved with this last dye is comparable with that of the unsubstituted indolenine-based VG1, for which a PCE of 4.7% (J_{sc} = 10.4 mA/cm^2, V_{oc} = 642 mV and ff = 72%) is registered. In any case, the central substituted dyes are always less efficient than the corresponding unsubstituted ones. Moreover, they follow the same trend both for indolenine- and benzoindolenine-based squaraines (VG1 > VG3 > VG2 and VG10 > VG12 > VG11).

Table 1. J-V characteristics for VG2-C8, VG3-C8, VG11-C8, VG12-C8 sensitized solar cells measured under standard A.M. 1.5G illumination (100 mW/cm^2). The values are compared to the benchmark C106 ruthenium dye [2] and to VG1-C8 [10] and VG10-C8 [11] using the same electrolyte composition.

Dye	V_{oc} (mV)	J_{sc} (mA/cm^2)	FF	η (%)
VG1	642	10.4	0.72	4.7
VG2	560	4.7	0.77	2.1
VG3	584	7.0	0.75	3.1
VG10	655	14.0	0.69	6.6
VG11	587	5.3	0.76	2.5
VG12	599	10.8	0.71	4.6
C106	660	18.4	0.69	8.6

In good agreement with the measured short-circuit current density, the IPCE spectra of the corresponding devices are reported in Figure 5b. The IPCEs of the non-substituted VG1 and VG10 are characterized by a broad and lower band in the blue region (S2) and a strong photo-conversion region between 550 and 750 nm (S1), with a maximum around 70%, according to [10,11]. Regardless of the structure, all the new four squaraines show an increased IPCE in the blue region (380–500 nm) and a noticeable decrease for S1 transition, together with a bathocromic shift. Differently from solution (Figure 3), in photovoltaic devices these two transitions are relatively comparable in terms of quantum efficiency. This suggests that S2 transition is more efficient at converting photons to electrons than the so-called S1 transition. More in detail, the central functionalization results in a 50 nm shift, comparing the non-functionalized squaraines (VG1 and VG10) with the dicyanovinyl substituted ones (VG2 and VG11), in agreement with the results reported by Maeda's and Han's groups for non-symmetrical squaraines [13,16]. On the contrary, replacing the dicyanovinyl group with a cyano-butyl-ester central unit (VG2 → VG3) slightly influences the absorption wavelength, but doubles the incident photon-to-electron conversion efficiency (from 23% at 710 nm to 41% at 715 nm). The same behavior is observed for benzo-indolenine squaraines VG11 → VG12 (from 25% at 730 nm to 51% at 740 nm), for which the π-conjugation extension also affords a quantum efficiency enhancement with a bathochromic shift of ca. 25 nm, with respect to VG2 and VG3. This huge enhancement is observed here for the first time, demonstrating that the electron withdrawing effect of the central functionalization seems to be detrimental for cell efficiency. However, it allows a bathochromic shift of the absorption maximum and an increase of the panchromatic response.

In order to gain insight into the relationship between the squaraine structures and the interfacial charge recombination vs. transport and distribution vs. energy of the intra-bandgap surface traps in TiO_2, electrochemical impedance spectroscopy (EIS) has been performed on the four new dyes to monitor ms to s time scale charge transfer processes. In darkness, the control of the quasi-Fermi level position inside the bandgap of the sensitized TiO_2 is achieved by applying an external bias voltage, between −0.7 V to −0.4 V. The resulting Nyquist spectra registered down to 100 mHz were adjusted using the mesoporous electrode transmission line model derived by Bisquert to the case of dye-sensitized solar cells operation [25].

EIS investigations are relatively powerful as they allow one to extract three key parameters governing the performance of the device: (i) the electron lifetime (τ_e) referring to the dynamic of electron recombination (Equation (1)); (ii) the electron collection time (τ_t) providing how fast the electron is transported through the mesoscopic TiO_2 network (Equation (2)) and (iii) the cell chemical capacitance (C_μ) (Equation (3)). The two first kinetic parameters are determined from the transmission line model by applying the following equations:

$$\tau_e = R_{ct,TiO2}\, C_\mu \quad (1)$$

$$\tau_t = R_{t,TiO2}\, C_\mu \quad (2)$$

where $R_{ct,TiO2}$ and $R_{t,TiO2}$ stands for the charge transfer resistance between electron populating the anatase TiO_2 and the redox acceptor I_3^- and the electron transport resistance throughout the nanoparticles network, respectively. In this work, we are assuming that the cell capacitance corresponds to the chemical capacitance of the anatase TiO_2, therefore the chemical capacitance of the FTO is negligible within the applied voltage window of −0.4 to −0.7 V. The capacitance of the film starts rising exponentially when TiO_2 particles become conductive enough. This exponential rise is a typical behavior of the chemical capacitance of TiO_2 that is related to the total density of carriers (n), following the expression (Equation (3)):

$$C_\mu = \frac{e^2}{kT} n \quad (3)$$

where e is the absolute elementary charge, k is Boltzmann's constant and T is the temperature.

The term n is an important feature to gain insight on the electron transport mechanism as $n \approx (n_{CB})^\beta$, where $\beta = 1$ if electrons are populating the conduction band. This value lies between 0.2 and 0.3 in dye-sensitized solar cells, indicating that electrons are not free in the conduction band but are rather populating surface intra-bandgap trap states for which the distribution follows a single exponential [26].

Using rigorously the same electrolyte and same photo-anode structure, we gathered in Figure 6 the evolution in the distribution and energy of the trap states located below the conduction band of TiO_2 depending on the type of dye.

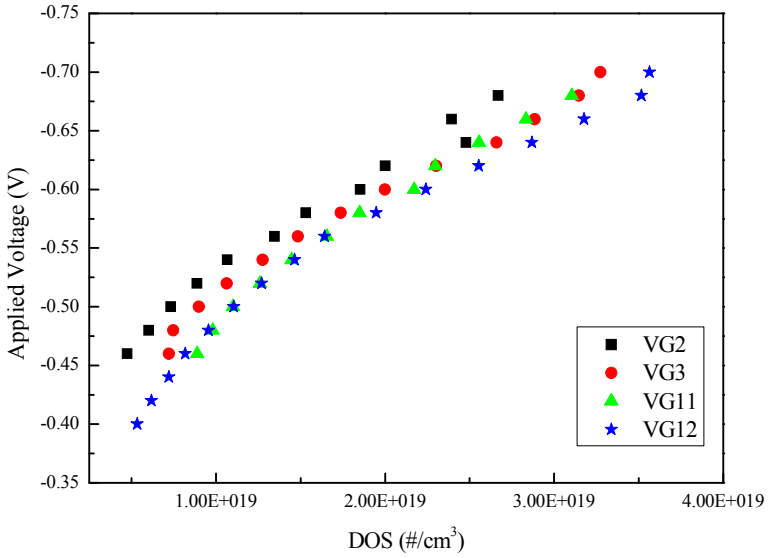

Figure 6. Energetic distribution as a function of Density of State (DOS) for devices including VG2-C8, VG3-C8, VG11-C8 and VG12-C8 dyes.

Note that the density of states (DOS) has been determined from the cell capacitance value, dominated by the chemical capacitance of TiO_2, using the following equation:

$$\mathrm{DOS}\,[\#/\mathrm{cm}^3] = \frac{6.24\cdot 10^{18}\,C_\mu}{L\,(1-p)} \quad (4)$$

where L corresponds to the film thickness and p to the photo-anode porosity [27].

The obtained results show that the structure of dye influences the energy of the traps by about 50 mV amplitude while they have no or little influence in their distribution. This tends to suggest that the four new dyes compared in this study have different dipole moment across the interface dye/TiO_2 as a result from either different molecular polarity and/or owing to a different molecular arrangement when anchored to the TiO_2's surface [28]. The modification of the central core unit has only little effect on the energy of the traps if we compare VG2 vs. VG3 and VG11 vs. VG12. However, this is different for the extension of π-conjugation in the anchoring group for which it gives rise to a more noticeable downshift in the energy of the traps. From these results, we can conclude that molecular arrangement of these squaraine dyes on TiO_2 takes place with the indolenine or benzoindolenine close to the TiO_2's surface and the group functionalizing the central squaraine core unit pointing towards the electrolyte. This would be perfectly consistent with the bidentate mode of the symmetrical squaraine dyes reported in the case of VG1 [10] and with the adopted spatial geometry of these dyes where either the dicyanovinyl or the cyano-ester is positioned oppositely than the indolenine or benzoindolenine acceptor units.

The impedance results describing the evolution of electron lifetime and electron transport time are reported in Figure 7 as a function of the chemical potential. This interpretation allows a direct comparison of the effect of the molecular dye on the charge collection vs. recombination (i.e., collection efficiency) for the same built-in charges in TiO_2. Comparing with the chemical capacitance avoids the additional effect of trap energy shifting which will also influence the dynamic of electron recombination and their transport.

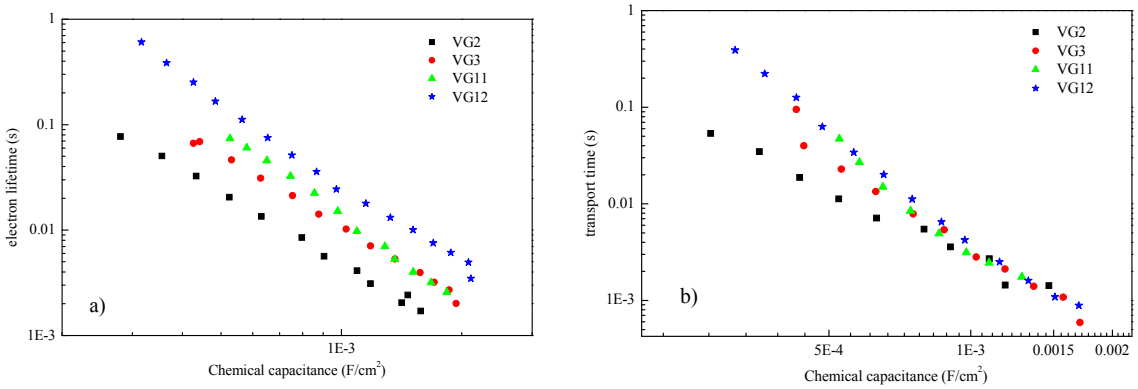

Figure 7. (**a**) Evolution of electron lifetime (τ_e); (**b**) transport time (τ_{tr}) as a function of device chemical capacitance (C_μ) for VG2-C8, VG3-C8, VG11-C8 and VG12-C8 dyes.

As for the energy of the traps, electron lifetime and charge collection time they are drastically influenced by the dye structure. The most blatant difference stems from the electron lifetime where the impedance shows that extending the π-conjugation in the anchoring ligand reduces recombination by three- to four-fold. This is in good agreement with a previous report on a D-π-A organic dye for which going from triphenylamine to trinaphthylamine results in an increase in the electron lifetime of the device [29]. Going from dicyanovinyl to the cyano-ester also allows one to enhance the electron lifetime by about two to three times, depending on the cell capacitance value. As a result, the molecular development from VG2 to VG12 leads to a reduction of the recombination rate by almost one order of magnitude. This explains why the photovoltage obtained with VG12 is the greatest compared to

the other VG2, VG3 and VG11 dyes. We can hypothesize that replacing the dicyanovinyl group by the cyano-ester unit increases the dye monolayer steric hindrance, hampering the tri-iodide from approaching the TiO_2 surface and the electron rich anchoring units, which seems to play a role in the recombination process according to our experimental evidences. The fact that the slope of electron lifetime is relatively unmodified by the structure of dye indicates that the electron recombination path is expected to be the same regardless of the dye's structure. As one could anticipate, the effect of the dye on the electron transport is less manifest, especially at higher charge carrier concentration ($>10^{-3}$ F/cm^2 or $>1.7\cdot 10^{19}$ #/cm^3) for which the transport time becomes independent of the structure of the dye (Figure 7b). At lower carrier concentration, the central core unit has little impact on the mechanism of electron transport by contrast to the anchoring group for which the indolenine seems more efficient than the benzoindolenine counterpart. This experimental evidence gives an additional credit to the aforementioned discussion regarding the influence of the dye geometry on the chemical capacitance of TiO_2. These results suggest that when the electron is deeply trapped inside the bandgap, the dye influences the trapping/detrapping energy; by contrast, when the electron is located closer to the bottom of the conduction band, its mobility (by multiple trapping/detrapping mechanism [30]) will become more governed by the density and energy of the free traps located nearby.

Extracted from the two antagonist kinetic pathways reported in Figure 6, one can deduce the evolution of the charge collection efficiency (η_{coll}) of the sensitized TiO_2 electrodes by these four symmetric squaraine dyes (Figure 8). For this, the charge collection efficiency was determined using the following equation:

$$\eta_{coll} = \frac{1}{1 + \frac{\tau_{tr}}{\tau_e}} \quad (5)$$

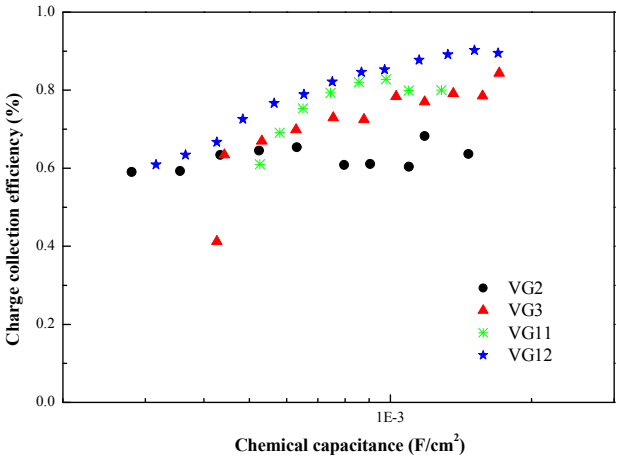

Figure 8. Evolution of the charge collection efficiency as a function of device chemical capacitance (C_μ) for VG2-C8, VG3-C8, VG11-C8 and VG12-C8 dyes.

As expected from the results depicted in Figure 8, the charge collection efficiency (η_{coll}) of VG12 is superior to the others, reaching a maximum of ca. 90% at high concentration of charge carriers. This improvement is ascribed to the combination between the most preponderant benzoindolenine unit and to a second plan the cyano-ester unit on the central moiety of the squaraine.

3. Materials and Methods

3.1. General Remarks

All the chemicals were purchased from Sigma Aldrich (Milan, Italy), except otherwise stated. The 2,3,3-trimethyl-3*H*-indole-5-carboxylic acid was supplied by Intatrade Chemicals GmbH (Muldestausee, Germany), and was used without any further purification. All microwave reactions were performed in a single-mode Biotage Initiator 2.5 (Biotage, Uppsala, Sweden). TLC was performed

on silica gel 60 F254 plates using DCM and methanol (90:10) as eluents. Column chromatography was performed on a Biotage Isolera Flash purification system. ^{1}H-NMR (200 MHz) spectra were recorded on an Avance 200 NMR instrument (Bruker, Billerica, MA, USA) in DMSO-d_6 using the residual DMSO signal as a reference.

3.2. Synthetic Procedures

The intermediates 4-(dimethylamino)pyridin-1-ium 3-(dicyanomethylene)-2-ethoxy-4-oxocyclobut-1-enolate (**1**) [18,31], 5-carboxy-2,3,3-trimethyl-1-octyl-3*H*-indol-1-ium iodide (**3**) [10], 7-carboxy-1,1,2-trimethyl-3-octyl-1*H*-benzo[e]indol-3-ium iodide (**4**) [11] were synthesized as previously reported in the literature.

3.2.1. 4-(Dimethylamino)pyridin-1-ium (*Z*)-3-(1-cyano-2-oxo-2-propoxyethylidene)-2-ethoxy-4-oxo-cyclobut-1-enolate (**2**) [32]

3,4-Diethoxy-3-cyclobutene-1,2-dione (1 mL, 6.8 mmol), butyl cyanoacetate (0.94 mL, 6.6 mmol), 4-(dimethylamino)pyridine (DMAP) (0.83 g, 6.8 mmol) and toluene (100 mL) are mixed and stirred for 90 min at room temperature and at reflux for 3 h. After cooling down, no precipitate is formed but two phases are evident: a brown solution at the bottom and a yellow one at the top. The two phases are separated, distilled and petroleum ether is added several times to wash the solid obtained from the brown phase to get intermediate **2** as a yellow powder (940 mg, yield = 83%). ^{1}H-NMR: (200 MHz, DMSO) δ: 8.20 (d, 2H), 6.96 (d, 2H), 4.62 (q, 2H), 3.93 (t, 2H), 3.17 (s, 6H), 1.52 (m, 2H), 1.29 (m, 5H), 0.88 (t, 3H).

3.2.2. VG2-C8

5-Carboxy-2,3,3-trimethyl-1-octyl-3*H*-indol-1-ium iodide (**3**, 638 mg, 1.44 mmol), 4-(dimethyl-amino)pyridin-1-ium 3-(dicyanomethylene)-2-ethoxy-3-oxocyclobut-1-enolate (**1**, 225 mg, 0.72 mmol) and toluene/*n*-butanol (1:1, 3 mL) were introduced in a microwave vial and heated at 155 °C for 30 min until TLC and UV showed reaction completion. After solvent evaporation, the crude product was crystallized in butanol and washed with hot acetone to obtain VG2-C8 as dark red powder (392 mg, yield = 72%). ^{1}H-NMR (DMSO-d_6): δ = 8.02 (m, 4H), 7.52 (d, 2H), 6.40 (s, 2H), 4.06 (m, 4H), 1.71 (s, 12H), 1.30–1.20 (m, 24H), 0.84 (m, 6H).

3.2.3. VG3-C8

5-Carboxy-2,3,3-trimethyl-1-octyl-3H-indol-1-ium iodide (**3**, 500 mg, 1.13 mmol), 4-(dimethyl-amino)pyridin-1-ium(*Z*)-3-(2-butoxy-1-cyano-2-oxoethylidene)-2-ethoxy-4-oxocyclobut-1-enolate (**2**, 190 mg, 0.49 mmol) and pyridine/*n*-butanol (1:1, 5 mL) were reacted in the MW oven at 155 °C for 15 min to obtain a precipitate which was filtered and crystallized with 0.5% CH_3COOH in ethanol. VG3-C8 is thus obtained as a dark green powder (216 mg, yield = 53%). ^{1}H-NMR (DMSO-d_6): δ = 8.04 (s, 2H), 7.98 (d, 2H), 7.60 (s, 1H), 7.46 (m, 2H), 6.82 (s, 1H), 4.09 (m, 6H), 1,72–1.57 (m, 18H), 1.46–1.21 (m, 22H), 0.92 (t, 3H), 0.82 (m, 6H).

3.2.4. VG11-C8

7-Carboxy-1,1,2-trimethyl-3-octyl-1*H*-benzo[e]indol-3-ium iodide (**4**, 0.2 g, 0.4 mmol), 4-(dimethylamino)pyridin-1-ium 3-(dicyanomethylene)-2-ethoxy-4-oxocyclobut-1-enolate (**1**) (63 mg, 0.2 mmol) and toluene/*n*-butanol (1:1, 1.5 mL) were introduced in a microwave vial and heated at 155 °C for 15 min until TLC and UV showed reaction completion. Solvents were then removed by evaporation and the crude product was washed with hot acetone, put at −20 °C for 30 min and filtered off to get a red solid of VG11-C8 (40 mg, yield = 23%). ^{1}H-NMR (DMSO-d_6): δ = 8.71 (s, 2H), 8.40 (d, 2H), 8.28 (d, 2H), 8.10 (d, 2H), 7.85 (d, 2H), 6.44 (s, 2H), 4.20 (m, 4H), 1.98 (s, 12H), 1.75–1.22 (m, 12H), 0.82 (m, 6H).

3.2.5. VG12-C8

7-Carboxy-1,1,2-trimethyl-3-octyl-1*H*-benzo[e]indol-3-ium iodide (**4**, 0.8 g, 1.6 mmol), 4(dimethylamino)pyridin-1-ium(*E*)-3-(2-butoxy-1-cyano-2-oxoethylidene)-2-ethoxy-4-oxocyclobut-1-enolate (**2**, 314 mg, 0.8 mmol) and toluene/*n*-butanol (1:1, 6 mL) were introduced in a microwave vial and heated at 155 °C for 15 min until TLC and UV showed reaction completion. The reaction solution was dropped in 250 mL of diethyl ether while stirring to obtain a purple precipitate that was removed by filtration. The solution was distilled and the crude material was redissolved in CH_2Cl_2/CH_3OH and purified on a silica samplet to get a brown solid which was further washed with CH_2Cl_2 to get pure VG12-C8 (98 mg , yield = 13%). ^{1}H-NMR (DMSO-d_6): δ = 8.69 (s, 2H), 8.37 (d, 2H), 8.25 (d, 2H), 8.08 (d, 2H), 7.82 (m, 2H), 7.63 (s, 1H), 6.85 (s, 1H), 4.18 (m, 4H), 4.10 (m, 2H), 1.99 (s, 12H), 1.76 (m, 4H), 1.65 (m, 3H), 1.42–1.22 (m, 20H), 0.94 (t, 4H), 0.82 (m, 6H).

3.3. Spectroscopic Measurements

Absorption spectra of new dyes were obtained by UV-Vis spectroscopy (Cary 300 Bio, Varian, Santa Clara, CA, USA) from 300 to 800 nm, using quartz cuvettes (1 cm pathway length). Absorption spectra were also recorded in different solvents to evaluate solvatochromism.

Steady-state fluorescence measurements were recorded using a Fluorolog 3 spectrofluorimeter (Horiba Jobin Yvon, Edison, NJ, USA). The excitation wavelength was set on the squaraine shoulder. The range for fluorescence emission recording was from 680 to 850 nm. The quantum yield was determined combining Quanta-φ with Fluorolog 3. The reported quantum yields are the average of the values obtained after three measurements using three different dye solutions.

Fluorescence lifetimes were obtained using a NanoLED source (636 nm, Horiba Jobyn Ivon, Edison, NJ, USA) and a TBX04 single photon counting detector (Horiba Jobin Yvon, Edison, NJ, USA). The same solutions used for quantum yield determination were used. The data were fitted to a single exponential function giving the lifetime.

3.4. Cyclic Voltammetry Measurements

Cyclic voltammetry was performed using a Bio-Logic SP150 (Bio-Logic, Claix, France) in DMF with 0.1 M $TBAPF_6$ as supporting electrolyte. A conventional three-electrode system was used with a glassy carbon electrode (1 mm diameter) as working electrode; a platinum wire was used as counter electrode and a Ag/Ag^+, $TBAPF_6$ 0.1 M in DMF as reference electrode. CVs were obtained at a scan rate of 100 mV/s. Ferrocene was used as internal reference and added in the last potential scans.

3.5. Computational Studies

We employed the LC-ωPBE functional which has been proven to be quite accurate for the description of molecular properties, including long range charge-transfer [33]. In all calculations the 6-31+G(d,p) basis set was used and solvent effects were included using the polarizable (PCM). All calculations were performed using the Gaussian09 software [34].

3.6. Solar Cell Fabrication and Characterization

A 8 µm TiO_2 transparent layer, composed by 20 nm anatase nanoparticles (synthesized as previously reported in literature [35]), and a 5 µm scattering layer of TiO_2 (Ti-Nanoxide R/SP, Solaronix, Aubonne, Switzerland) were screen printed onto a fluorine-doped tin oxide (FTO) conductive glass (Nippon Sheet Glass NSG 10, 3.2 mm thick, 10 Ω/cm, Pilkington, Tokyo, Japan). The thickness was measured with a Dektak XT profilometer (Bruker, Karlsruhe, Germany). The screen printed electrodes were heat treated under air following a temperature ramp up to 500 °C to decompose the ethyl cellulose porogen and to ensure good electronic contacts between the particles and also with FTO. The different dye solutions were prepared in ethanol with a concentration of 0.1 mM. 10 mM of chenodeoxycholic acid (CDCA) was added to prevent dye aggregation. The photoelectrodes were

thermal treated at 500 °C with a hot gun (Leister, Obwald, Switzerland), then cooled down and dipped into the dye solution for 5 h in dark condition at room temperature. The counter electrodes were made of platinized FTO (TEC7, Pilkington, Tokyo, Japan, 3 mm thick, 7 Ω/cm^2). The two electrodes were assembled using Surlyn® (25 µm, Solaronix, Aubonne, Switzerland) thermofusing polymer. The electrolyte was composed of: 1 M 1,3-dimethylimidazolium iodide synthesized according to the literature [36], 0.03 M I_2 (⩾99.8%) , 0.05 M LiI (99%, Alfa Aesar, Karlsruhe, Germany), 0.1 M guanidinium thiocyanate (99%, Alfa Aesar, Karlsruhe, Germany) and 0.5 M 4-*tert*-butylpyridine (96%) in 15/85 (v/v) mixture of valeronitrile (99%, Alfa Aesar) and acetonitrile (99.9%, VWR). The photovoltaics properties were measured under A.M. 1.5G conditions (P_{ill} = 100 mW/cm^2) using 3A class Newport SOL3A sun simulator equipped with a 450 W Xenon arc lamp and a 1.5G air mass filter, connected to a digital source meter (Keithley 2402, Keithley Instrument Inc., Berkshire, United Kingdom). The J-V characteristics were recorded from open-circuit to short-circuit condition. For this, the devices of 0.148 cm^2 (square geometry) were masked by a black tape of 1 mm larger aperture than TiO_2. The Incident Photon-to-current Conversion Efficiency (IPCE) was measured with a Newport IQE-200 (Newport Corporation, Santa Clara, CA, USA) equipped with a 250 W quartz tungsten halogen lamp. The device was biased with continuous white light chopped at 10 Hz frequency.

3.7. EIS Measurements

Electrochemical Impedance Spectroscopy (EIS) was performed using a Bio-Logic VMP2 impedancemeter. The spectra were collected in dark conditions and in thermostated environment at 25 °C. The impedance spectra were acquired between 10^5 and 0.1 Hz by superimposing a small sinusoidal voltage perturbation of ΔE = 10 mV. The imposed voltage was scanned from −0.7 V to −0.3 V. The collected data were adjusted by using Zview software with the transmission line model as an electrical equivalent circuit [25].

4. Conclusions

Novel *cis*-configured central functionalized symmetric squaraine dyes have been synthesized and characterized spectroscopically and electrochemically, in order to register the DSCs' properties in function of the dicyanovinyl and cyano-ester group substitution on the core and the elongation of the π-conjugation. As expected, the introduction of the cyano-butyl-ester group caused a slight bathochromic shift in comparison to the dicyano-substituted dye. More interestingly, it doubled the incident photon-to-electron conversion efficiency for both systems (indolenine- and benzoindolenine-based squaraines).

The highest efficiency of 4.6% with 10.8 mA/cm^2 photocurrent was obtained with the VG12-C8 dye bearing a cyano-ester group on the squaraine central core and two benzoindolenine units with a photoconversion onset that reaches 51% maximum IPCE at 740 nm with a tail of conversion up to 800 nm. Electrochemical impedance spectroscopy gave evidence that going from dicyanovinyl to cyano-ester unit and from indolenine to benzoindolenine affords to increase the charge collection efficiency, which has to be put on the credit of the increase by almost one order of magnitude in the electron lifetime.

The huge enhancement in IPCE and cell efficiency going from dicyanovinyl to cyano-ester group substitution was observed here for the first time, demonstrating that the electron withdrawing effect of the central functionalization seems to be detrimental for cell efficiency. In general, non-substituted squaraines showed better cell efficiencies than central substituted ones. In the future, other groups with a lower electron withdrawing effect or bulky groups could be investigated for a real improvement of cell performances.

Supplementary Materials: The following are available online at www.mdpi.com/1996-1073/9/7/486/s1. Figure S1: Synthetic procedures of VG2-C8, VG3-C8, VG11-C8, VG12-C8 and their intermediates. Experimental conditions: (i) toluene, 30 min, RT; (ii) toluene/BuOH, MW, 30 min, 155 °C; (iii) pyridine/BuOH, MW, 15 min, 155 °C; (iv) toluene, 90 min, RT; 3 h reflux; (v) toluene/BuOH, MW, 15 min, 155 °C. Figure S2: ^{1}H NMR of intermediate 1. Figure S3: ^{1}H NMR of intermediate 2. Figure S4: ^{1}H NMR of VG2-C8. Figure S5: ^{1}H NMR of VG3-C8. Figure S6: ^{1}H NMR of VG11-C8. Figure S7: ^{1}H NMR of VG12-C8. Figure S8: Cyclic voltammograms of VG2-C8, VG3-C8, VG11-C8 and VG12-C8 at scan rate 100 mV·s^{-1}, 2nd scan is shown. Figure S9: Upper panel HOMO, lower panel LUMO of the four dyes. In all cases the HOMO has a significant contribution from the substituent orbitals, while the LUMO is typical of squaraines. Table S1: Absorption maxima (λ_{max}) in different solvents and logε in ethanol for VG2-C8, VG3-C8, VG11-C8 and VG12-C8. Table S2: Emission maxima, Stokes shift, HOMO-LUMO energy gaps, lifetimes and quantum yields for VG2 and VG3 in different solvents. Table S3: Emission maxima, Stokes shift, HOMO-LUMO energy gaps, lifetimes and quantum yields for VG11 and VG12 in different solvents. Table S4: Vertical excitation energies (in nm) and oscillator strengths (in cm^{-1}), in parenthesis, of the functionalized squaraines, obtained from TD-DFT calculations. All calculations include the effect of tetrahydrofuran solvent by means of PCM.

Acknowledgments: The authors gratefully acknowledge financial support of the DSSCX project (PRIN 2010-2011, 20104XET32) from MIUR. R.B. acknowledges the CINECA award WASPET-HP10CK2XJ under the ISCRA initiative, for the availability of high performance computing resources and support.

Author Contributions: G. Viscardi and C. Barolo conceived and designed the molecules and the synthesis; S. Galliano, N. Barbero and A. Smarra performed the synthesis and the characterizations; R. Borrelli performed the computational calculations; V. Novelli and F. Sauvage prepared the photovoltaic devices and performed the photoelectrochemical and impedance analysis.

Conflicts of Interest: The authors declare no conflict of interest.

Abbreviations

The following abbreviations are used in this manuscript:

CV	cyclic voltammetry
DSCs	dye-sensitized solar cells
EIS	electrochemical impedance spectroscopy
FTO	fluorine-doped tin oxide
HOMO	highest occupied molecular orbital
LUMO	lowest unoccupied molecular orbital
MLCT	metal to ligand charge transfer
NIR	near infrared
PCE	power conversion efficiencies
TD-DFT	time-dependent density functional theory
TICT	twisted intramolecular charge transfer

References

1. Kakiage, K.; Aoyama, Y.; Yano, T.; Oya, K.; Fujisawa, J.; Hanaya, M. Highly-efficient dye-sensitized solar cells with collaborative sensitization by silyl-anchor and carboxy-anchor dyes. *Chem. Commun.* **2015**, *51*, 15894–15897. [CrossRef] [PubMed]
2. Cao, Y.; Bai, Y.; Yu, Q.; Cheng, Y.; Liu, S.; Shi, D.; Gao, F.; Wang, P. Dye-Sensitized Solar Cells with a High Absorptivity Ruthenium Sensitizer Featuring a 2-(Hexylthio)thiophene Conjugated Bipyridine. *J. Phys. Chem. C* **2009**, *113*, 6290–6297. [CrossRef]
3. Balasingam, S.K.; Lee, M.; Kang, M.G.; Jun, Y. Improvement of dye-sensitized solar cells toward the broader light harvesting of the solar spectrum. *Chem. Commun.* **2013**, *49*, 1471–1487. [CrossRef] [PubMed]
4. Yum, J.H.; Hagberg, D.P.; Moon, S.J.; Karlsson, K.M.; Marinado, T.; Sun, L.; Hagfeldt, A.; Nazeeruddin, M.K.; Grätzel, M. A light-resistant organic sensitizer for solar-cell applications. *Angew. Chem. Int. Ed.* **2009**, *48*, 1576–1580. [CrossRef] [PubMed]
5. Wang, Z.S.; Koumura, N.; Cui, Y.; Takahashi, M.; Sekiguchi, H.; Mori, A.; Kubo, T.; Furube, A.; Hara, K. Hexylthiophene-functionalized carbazole dyes for efficient molecular photovoltaics: Tuning of solar-cell performance by structural modification. *Chem. Mater.* **2008**, *20*, 3993–4003. [CrossRef]
6. Feldt, S.M.; Gibson, E.A.; Gabrielsson, E.; Sun, L.; Boschloo, G.; Hagfeldt, A. Design of organic dyes and cobalt polypyridine redox mediators for high-efficiency dye-sensitized solar cells. *J. Am. Chem. Soc.* **2010**, *132*, 16714–16724. [CrossRef] [PubMed]

7. Saccone, D.; Galliano, S.; Barbero, N.; Viscardi, G.; Barolo, C. Polymethine dyes in photovoltaics: A structure-properties relationship. *Eur. J. Org. Chem.* **2016**, *2016*, 2244–2259. [CrossRef]
8. Park, J.; Viscardi, G.; Barolo, C.; Barbero, N. Near-infrared sensitization in dye-sensitized solar cells. *Chimia* **2013**, *67*, 129–135. [CrossRef] [PubMed]
9. Tatikolov, A.S.; Costa, S.M. Photophysical and aggregation properties of a long-chain squarylium indocyanine dye. *J. Photochem. Photobiol. A Chem.* **2001**, *140*, 147–156. [CrossRef]
10. Park, J.; Barolo, C.; Sauvage, F.; Barbero, N.; Benzi, C.; Quagliotto, P.; Coluccia, S.; di Censo, D.; Grätzel, M.; Nazeeruddin, M.K.; et al. Symmetric vs. asymmetric squaraines as photosensitisers in mesoscopic injection solar cells: A structure-property relationship study. *Chem. Commun.* **2012**, *48*, 2782–2784. [CrossRef] [PubMed]
11. Park, J.; Barbero, N.; Yoon, J.; Dell'Orto, E.; Galliano, S.; Borrelli, R.; Yum, J.-H.; di Censo, D.; Grätzel, M.; Nazeeruddin, M.K.; et al. Panchromatic symmetrical squaraines: A step forward in the molecular engineering of low cost blue-greenish sensitizers for dye-sensitized solar cells. *Phys. Chem. Chem. Phys.* **2014**, *16*, 24173–24177. [CrossRef] [PubMed]
12. Beverina, L.; Ruffo, R.; Mari, C.M.; Pagani, G.A.; Sassi, M.; De Angelis, F.; Fantacci, S.; Yum, J.-H.; Grätzel, M.; Nazeeruddin, M.K. Panchromatic cross-substituted squaraines for dye-sensitized solar cell applications. *Chem. Sus. Chem.* **2009**, *2*, 621–624. [CrossRef] [PubMed]
13. Maeda, T.; Mineta, S.; Fujiwara, H.; Nakao, H.; Yagi, S.; Nakazumi, H. Conformational effect of symmetrical squaraine dyes on the performance of dye-sensitized solar cells. *J. Mater. Chem. A* **2013**, *1*, 1303–1309. [CrossRef]
14. Qin, C.; Numata, Y.; Zhang, S.; Islam, A.; Yang, X.; Sodeyama, K.; Tateyama, Y.; Han, L. A near-infrared *cis*-configured squaraine Co-sensitizer for high-efficiency dye-sensitized solar cells. *Adv. Funct. Mater.* **2013**, *23*, 3782–3789. [CrossRef]
15. Rao, G.H.; Venkateswararao, A.; Giribabu, L.; Singh, S.P. Near-infrared unsymmetrical blue and green squaraine sensitizers. *Photochem. Photobiol. Sci.* **2016**, *15*, 287–296. [CrossRef] [PubMed]
16. Qin, C.; Numata, Y.; Zhang, S.; Yang, X.; Islam, A.; Zhang, K.; Chen, H.; Han, L. Novel near-infrared squaraine sensitizers for stable and efficient dye-sensitized solar cells. *Adv. Funct. Mater.* **2014**, *24*, 3059–3066. [CrossRef]
17. Zhang, K.; Qin, C.; Yang, X.; Islam, A.; Zhang, S.; Chen, H.; Han, L. High-performance, transparent, dye-sensitized solar cells for see-through photovoltaic windows. *Adv. Energy Mater.* **2014**, *4*, 1–7. [CrossRef]
18. Barbero, N.; Magistris, C.; Park, J.; Saccone, D.; Quagliotto, P.; Buscaino, R.; Medana, C.; Barolo, C.; Viscardi, G. Microwave-Assisted Synthesis of Near-Infrared Fluorescent Indole-Based Squaraines. *Org. Lett.* **2015**, *17*, 3306–3309. [CrossRef] [PubMed]
19. Volkova, K.D.; Kovalska, V.B.; Tatarets, A.L.; Patsenker, L.D.; Kryvorotenko, D.V.; Yarmoluk, S.M. Spectroscopic study of squaraines as protein-sensitive fluorescent dyes. *Dyes Pigment.* **2007**, *72*, 285–292. [CrossRef]
20. Mayerhöffer, U.; Fimmel, B.; Würthner, F. Bright near-infrared fluorophores based on squaraines by unexpected halogen effects. *Angew. Chem. Int. Ed.* **2012**, *51*, 164–167. [CrossRef] [PubMed]
21. Tatarets, A.L.; Fedyunyaeva, I.A.; Terpetschnig, E.; Patsenker, L.D. Synthesis of novel squaraine dyes and their intermediates. *Dyes Pigment.* **2005**, *64*, 125–134. [CrossRef]
22. Borrelli, R.; Ellena, S.; Barolo, C. Theoretical and experimental determination of the absorption and emission spectra of a prototypical indolenine-based squaraine dye. *Phys. Chem. Chem. Phys.* **2014**, *16*, 2390–2398. [CrossRef] [PubMed]
23. Benzi, C.; Bertolino, C.A.; Miletto, I.; Ponzio, P.; Barolo, C.; Viscardi, G.; Coluccia, S.; Caputo, G. The design, synthesis and characterization of a novel acceptor for real time polymerase chain reaction using both computational and experimental approaches. *Dyes Pigment.* **2009**, *83*, 111–120. [CrossRef]
24. Magistris, C.; Martiniani, S.; Barbero, N.; Park, J.; Benzi, C.; Anderson, A.; Law, C.; Barolo, C.; O'Regan, B. Near-infrared absorbing squaraine dye with extended conjugation for dye-sensitized solar cells. *Renew. Energy* **2013**, *60*, 672–678. [CrossRef]
25. Fabregat-Santiago, F.; Bisquert, J.; Garcia-Belmonte, G.; Boschloo, G.; Hagfeldt, A. Influence of electrolyte in transport and recombination in dye-sensitized solar cells studied by impedance spectroscopy. *Sol. Energy Mater. Sol. Cells* **2005**, *87*, 117–131. [CrossRef]

26. Fabregat-Santiago, F.; Mora-Seró, I.; Garcia-Belmonte, G.; Bisquert, J. Cyclic voltammetry studies of nanoporous semiconductors. Capacitive and reactive properties of nanocrystalline TiO_2 electrodes in aqueous electrolyte. *J. Phys. Chem. B* **2003**, *107*, 758–768. [CrossRef]
27. O'Regan, B.C.; Durrant, J.R.; Sommeling, P.M.; Bakker, N.J. Influence of the $TiCl_4$ Treatment on Nanocrystalline TiO_2 Films in Dye-Sensitized Solar Cells 2 Charge Density, Band Edge Shifts, and Quantification of Recombination Losses at Short Circuit. *J. Phys. Chem. C* **2007**, *111*, 14001–14010. [CrossRef]
28. De Angelis, F.; Fantacci, S.; Selloni, A.; Grätzel, M.; Nazeeruddin, M.K. Influence of the sensitizer adsorption mode on the open-circuit potential of dye-sensitized solar cells. *Nano Lett.* **2007**, *7*, 3189–3195. [CrossRef] [PubMed]
29. Olivier, C.; Sauvage, F.; Ducasse, L.; Castet, F.; Grätzel, M.; Toupance, T. Fine-tuning of triarylamine-based photosensitizers for dye-sensitized solar cells. *Chem. Sus. Chem.* **2011**, *4*, 731–736. [CrossRef] [PubMed]
30. Bisquert, J.; Fabregat-Santiago, F.; Mora-Sero, I.; Garcia-Belmonte, G.; Gimenez, S. Electron Lifetime in Dye-Sensitized Solar Cells: Theory and Interpretation of Measurements. *J. Phys. Chem. C* **2009**, *113*, 17278–17290. [CrossRef]
31. Zubatyuk, R.I.; Baumer, V.N.; Tatarets, A.L.; Patsenker, L.D.; Shishkin, O.V. 4-(Dimethylamino)pyridmium 2-butoxy-3-dicyanomethylene-4-oxocyclobut-1-en-1-olate. *Acta Crystallogr. Sect. E Struct. Rep. Online* **2004**, *60*, o2252–o2254. [CrossRef]
32. Terpetschnig, E.A.; Patsenker, L.; Tatarets, A.; Fedyunyaeva, I.; Borovoy, I. Dyes and Fluorescent Compounds, Their Production and Use. International Patent WO 2003087052, 23 October 2003.
33. Vydrov, O.A.; Scuseria, G.E. Assessment of a long-range corrected hybrid functional. *J. Chem. Phys.* **2006**, *125*, 234109. [CrossRef] [PubMed]
34. Frisch, M.J.; Trucks, G.W.; Schlegel, H.B.; Scuseria, G.E.; Robb, M.A.; Cheeseman, J.R.; Scalmani, G.; Barone, V.; Mennucci, B.; Petersson, G.A.; et al. *Gaussian 09, Revision A*; Gaussian Inc.: Wallingford, CT, USA, 2009.
35. Ito, S.; Murakami, T.N.; Comte, P.; Liska, P.; Grätzel, C.; Nazeeruddin, M.K.; Grätzel, M. Fabrication of thin film dye sensitized solar cells with solar to electric power conversion efficiency over 10%. *Thin Solid Films* **2008**, *516*, 4613–4619. [CrossRef]
36. Oertel, A.M.; Ritleng, V.; Burr, L.; Chetcuti, M.J. Synthesis and Structural Characterization of Half-Sandwich Nickel Complexes Bearing Two Different N-Heterocyclic Carbene Ligands. *Organometallics* **2011**, *30*, 6685–6691. [CrossRef]